

Relations among Turbulent Fluctuations, Zonal Flows, and Transport Coefficients in Time Series Data of Gyrokinetic Simulations^{*)}

Kotaro FUJII¹⁾ and Masanori NUNAMI^{1,2)}

¹⁾Nagoya University, Furo-cho, Chikusa-ku, Nagoya 464-8601, Japan

²⁾National Institute for Fusion Science, 322-6 Oroshi-cho, Toki 509-5292, Japan

(Received 10 January 2022 / Accepted 24 February 2022)

The relations among turbulent amplitude, zonal-flow amplitude, and transport level are discussed for the time series data of nonlinear gyrokinetic simulations for magnetized toroidal plasmas. Since it was shown that the transport coefficient can be expressed as a function of the time-averaged turbulent fluctuation level and the zonal flow amplitude [M. Nunami *et al.*, Phys. Plasmas **20**, 092307 (2013)], we apply the results to a model function for the turbulent plasma transport coefficient to extend to a functional relation which includes not the time-averaged data but the time-series data of gyrokinetic simulations. We obtain a new functional relation to the turbulent fluctuations, the zonal-flow amplitudes, and the transport coefficients as a function of the input parameters of the gyrokinetic simulations such as plasma temperature gradients. It is also confirmed that the obtained functional relation can reduce relative error which is compared with the original function with time-averages.

© 2022 The Japan Society of Plasma Science and Nuclear Fusion Research

Keywords: turbulent transport, transport model, gyrokinetic simulation

DOI: 10.1585/pfr.17.2403030

1. Introduction

Anomalous transport plays an important role in fusion reactor plasmas. Therefore, it is necessary to understand the physical mechanisms of anomalous transport in magnetically confined fusion plasmas. Numerical simulations based on a gyrokinetic model for drift wave turbulence caused by microinstability, such as the ion temperature gradient (ITG) mode [1], have been performed with the aim of understanding anomalous transport mechanisms. Although quantitative evaluations of transport need simulation results under various conditions, the nonlinear gyrokinetic simulations of turbulent transport [2] entail huge computational costs, so that it is not practical to perform the simulations many times over. It has been tried to represent the transport level in terms of a simplified model to predict the level. For tokamak plasmas, some transport models such as the GLF23 [3], TGLF [4–6], and QuaLiKiz [7] have been proposed, but these models did not adapt to helical plasmas. For helical plasmas, a model function which predicts the ion heat diffusivity of nonlinear gyrokinetic simulation for Large Helical Device (LHD) plasmas was developed [8] by including the effect of zonal flows from a phenomenological viewpoint. In the model, using time-averages of turbulent amplitude \mathcal{T} and zonal flow amplitude \mathcal{Z} , the normalized ion transport coefficients

$\tilde{\chi}_i$ was represented by the function,

$$\langle \tilde{\chi}_i^{\text{Model1}} \rangle = \frac{C_1 \langle \mathcal{T} \rangle^\alpha}{1 + C_2 \sqrt{\langle \mathcal{Z} \rangle} / \langle \mathcal{T} \rangle}, \quad (1)$$

where \mathcal{T} and \mathcal{Z} are defined by using the squared potential fluctuation,

$$\mathcal{T} \equiv \frac{1}{2} \sum_{k_x, k_y \neq 0} \langle \langle |\delta\phi_{k_x, k_y}|^2 \rangle \rangle, \quad (2)$$

$$\mathcal{Z} \equiv \frac{1}{2} \sum_{k_x} \langle \langle |\delta\phi_{k_x, k_y=0}|^2 \rangle \rangle, \quad (3)$$

and (C_1, C_2, α) are determined by the nonlinear fitting. For the particle species of s , the electrostatic potential fluctuation is normalized as $\delta\phi = \phi / (T_s \rho_s / eR_0)$ with the temperature T_s , the Larmor radius ρ_s , and major radius R_0 . The Larmor radius is given by $\rho_s = v_{T_s} / \Omega_s$ by using the thermal velocity $v_{T_s} = \sqrt{T_s / m_s}$ and the gyrofrequency Ω_s . The time-average and flux-average are denoted by $\langle \dots \rangle$ and $\langle \langle \dots \rangle \rangle$, respectively, and (k_x, k_y) represent the radial and poloidal wavenumbers.

The work presented here is the structure of time series data of gyrokinetic simulations and a time-dependent functional relation, based on $\langle \tilde{\chi}_i^{\text{Model1}} \rangle$ for time series data of $\tilde{\chi}_i$, \mathcal{T} , and \mathcal{Z} . After the verification of nonlinear fitting, the new functional relation is compared with the previous function, $\langle \tilde{\chi}_i^{\text{Model1}} \rangle$ in order to examine its validity. Furthermore, we discuss an underestimation caused in the new functional relation.

author's e-mail: fuji.kohtar@nifs.ac.jp

^{*)} This article is based on the presentation at the 30th International Toki Conference on Plasma and Fusion Research (ITC30).

This paper is organized as follows. Details about the simulations performed this work are described in section 2. The results are presented in section 3, followed by a discussion in section 4 and a conclusion in section 5.

2. Gyrokinetic Simulation

In this work, we perform gyrokinetic Vlasov simulations of ITG turbulent transport with kinetic electrons by using the GKV code [9], which is one of the local flux-tube codes. The GKV code solves the electromagnetic gyrokinetic equation of the perturbed gyrocenter distribution function δf_{sk} [9–11],

$$\begin{aligned} & \left(\frac{\partial}{\partial t} - \frac{\mu}{m_s} \mathbf{b} \cdot \nabla B \frac{\partial}{\partial v_{\parallel}} \right) \delta f_{sk} \\ & + (v_{\parallel} \mathbf{b} \cdot \nabla + i v_{ds} \cdot \mathbf{k}_{\perp}) \left(\delta f_{sk} + \frac{q_s F_{Ms}}{T_s} \delta \phi J_{0sk} \right) \\ & + \frac{q_s F_{Ms}}{T_s} \left\{ \frac{\partial}{\partial t} J_{0sk} \delta A_{\parallel k} - i v_{*s} \cdot \mathbf{k}_{\perp} J_{0sk} \left(\delta \phi_k - \frac{v_{\parallel}}{c} \delta A_{\parallel k} \right) \right\} \\ & - \frac{c}{B_0} \sum_{\mathbf{k}'_{\perp} + \mathbf{k}''_{\perp} = \mathbf{k}_{\perp}} \mathbf{b} \cdot (\mathbf{k}'_{\perp} \times \mathbf{k}''_{\perp}) J_{0sk} \left(\delta \phi_k - \frac{v_{\parallel}}{c} \delta A_{\parallel k} \right) \\ & \times \left(\delta f_{sk} + \frac{q_s F_{Ms}}{T_s} \delta \phi J_{0sk} \right) \\ & = C_{sk}, \end{aligned} \quad (4)$$

and Poisson-Ampère equations,

$$\begin{aligned} & \left\{ k_{\perp}^2 + \frac{1}{\epsilon_0} \sum_s \frac{q_s^2 n_s}{T_s} (1 - \Gamma_{0sk}) \right\} \delta \phi_k \\ & = \frac{1}{\epsilon_0} \sum_s q_s \int d v^3 J_{0sk} \delta f_{sk}, \end{aligned} \quad (5)$$

$$k_{\perp}^2 \delta A_{\perp k} = \mu_0 \sum_s q_s \int d v^3 J_{0sk} v_{\parallel} \delta f_{sk}, \quad (6)$$

where $J_{0sk} = J_0(\rho_s k_{\perp})$ and $\Gamma_{0sk} = I_0(k_{\perp}^2 \rho_s^2) e^{-k_{\perp}^2 \rho_s^2}$ with zeroth-order Bessel function J_0 and zeroth-order modified Bessel function I_0 . In equation (5) and (6), B_0 , c , q_s are magnetic field strength on the magnetic axis, the speed of light, and the electric charge. The parallel velocity, v_{\parallel} , and the magnetic moment, $\mu = m_s v_{\perp}^2 / 2B$, are used as the velocity-space coordinates. The Maxwell distribution functions with density n_s are denoted by $F_{Ms} = n_s (m_s / 2\pi T_s)^{3/2} \exp(-m_s v_{\parallel}^2 / 2T_s - \mu B / T_s)$, and the collision term is C_s . The magnetic and diamagnetic drift velocities are represented by $v_{ds} = c \mathbf{b} / q_s B \times (\mu \nabla B + m_s v_{\parallel}^2 \mathbf{b} \cdot \nabla \mathbf{b})$ and $v_{*s} = c T_s \mathbf{b} / q_s B \times \nabla \ln F_{Ms}$. In this work, we assume that the ion and the electron temperatures are equal, $T_i = T_e$.

In order to obtain as much simulation data as possible, we have performed twenty-four nonlinear simulations totally with the parameters shown in Table 1. The grid sizes of 5D phase space are employed $(n_x, n_y, n_z, n_v, n_m) = (111, 30, 96, 64, 16)$ for $k_x, k_y, z, v_{\parallel}$, and μ .

Figure 1 shows the k_y spectrum of growth rates and real frequencies by assuming $\delta \phi_k(t) \propto \exp\{-i(\omega_r + i\gamma)t\}$. The real frequencies indicate an ion diamagnetic direction for negative and an electron diamagnetic direction for positive.

Table 1 Parameters used in the simulations. Here, the safety factor, the magnetic shear, the beta value, and the temperature and density scale length are represented by $q, \hat{s}, \beta, L_{Ts}$, and L_{ns} , respectively.

q	\hat{s}	β	R_0/L_{T_i}	R_0/L_{T_e}	R_0/L_{n_i}	R_0/L_{n_e}
1.4	0.8	5×10^{-4}	6.0 to 20.0	15.0	2.22	2.22

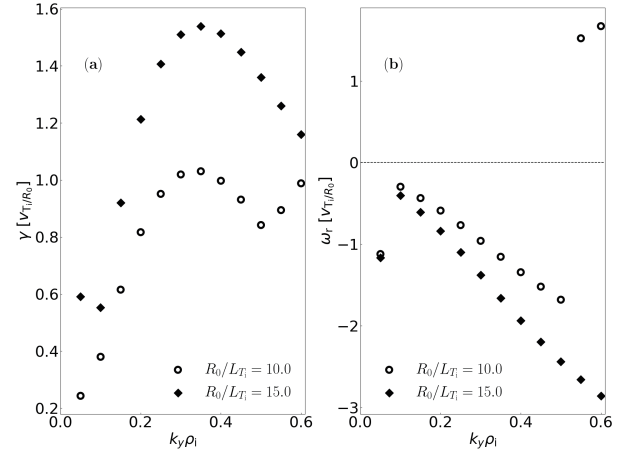


Fig. 1 The growth rate (a) and real frequency (b) against poloidal wavenumber for $R_0/L_{T_i} = 10.0$ and 15.0 . Here, $k_x = 0$.

From Fig. 1, it is found that the ITG mode is a dominant instability of this simulation, and the TEM mode is developed in a low ion temperature gradient.

3. The Structure of Time Series Data

In the previous work [8], the time-average of transport coefficients for each simulation condition were considered, and Model1 defined by Eq. (1) depended on the time-averages of, \mathcal{T} and \mathcal{Z} . Here, in order to clarify the time evolutions in the simulations, we focus on the structures of the time series data of the simulations in the space of the parameters, $(\mathcal{T}, \mathcal{Z}, \tilde{\chi}_i)$. As shown in Fig. 2 (a), it is found that the spatial structure varies only in a subspace for a condition. Therefore, we consider not only time-averages but also the time series to obtain the functional relation.

We examine the time-dependent functional relation for time series data of $\tilde{\chi}_i, \mathcal{T}$, and \mathcal{Z} with the functional relation defined by

$$\tilde{\chi}_i^{\text{Model12}}(t) = \frac{C_1^{(2)} \mathcal{T}(t)^{\alpha^{(2)}}}{1 + C_2^{(2)} \sqrt{\mathcal{Z}(t)/\mathcal{T}(t)}}. \quad (7)$$

The fitting parameters $(C_1^{(2)}, C_2^{(2)}, \alpha^{(2)})$ are determined by the Nelder-Mead simplex method [12] which does not require a derivative function. The objective function used for nonlinear fitting is $g(C_1^{(2)}, C_2^{(2)}, \alpha^{(2)})$, defined by

$$g(C_1^{(2)}, C_2^{(2)}, \alpha^{(2)}) = \sqrt{\frac{1}{N} \sum_{j=1}^N \left(\frac{\tilde{\chi}_i^{\text{Model12}}(t_j)}{\tilde{\chi}_i^{\text{GKV}}(t_j)} - 1 \right)^2}. \quad (8)$$

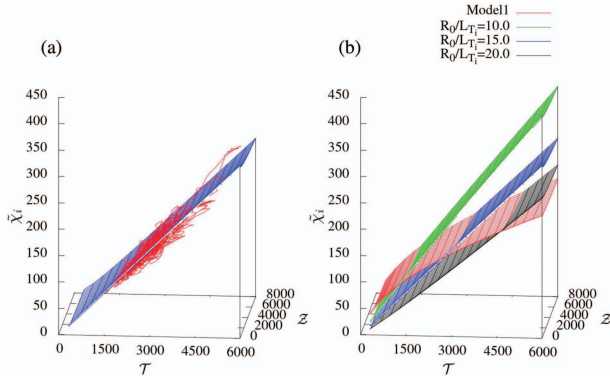


Fig. 2 The spatial structure of time series data of gyrokinetic simulation and function $\tilde{\chi}_i^{\text{Model12}}(t)$ surface. (a) Red line is time series data with $R_0/L_{T_i} = 15.0$, and blue curved surface indicates fitted function. (b) Surfaces for each simulation condition of R_0/L_{T_i} exist.

Here, the numbers j and N are the index number and the total number of the time-series data. The time series data obtained from gyrokinetic simulation is represented by $\tilde{\chi}_i^{\text{GKV}}(t)$.

Since the function $g(C_1^{(2)}, C_2^{(2)}, \alpha^{(2)})$ may have local minimum points, and the results of the concrete numerical optimization techniques depend on an initial set of several parameters, it is necessary to perform techniques for wide ranges of the initial parameters. Figure 3 shows the contours of the function $g(C_1^{(2)}, C_2^{(2)}, \alpha^{(2)})$ on (a) $C_2^{(2)}$ - $\alpha^{(2)}$ plane at $C_1^{(2)} = 6.0 \times 10^{-2}$, (b) the $C_1^{(2)}$ - $\alpha^{(2)}$ plane at $C_2^{(2)} = 6.0$, and (c) the $C_1^{(2)}$ - $C_2^{(2)}$ plane at $\alpha^{(2)} = 9.9 \times 10^{-1}$ for the case of $R_0/L_{T_i} = 15.0$, obtained by calculating $g(C_1^{(2)}, C_2^{(2)}, \alpha^{(2)})$ directly. In the figures it is confirmed that the optimization result by the Nelder-Mead simplex method, $(C_1^{(2)}, C_2^{(2)}, \alpha^{(2)}) = (6.0 \times 10^{-2}, 6.0, 9.9 \times 10^{-1})$, can exist in the global minimum point, (a) $(C_2^{(2)}, \alpha^{(2)}) = (6.0, 9.9 \times 10^{-1})$, (b) $(C_1^{(2)}, \alpha^{(2)}) = (6.1 \times 10^{-2}, 9.9 \times 10^{-1})$, and (c) $(C_1^{(2)}, C_2^{(2)}) = (6.0 \times 10^{-2}, 6.0)$. The nontrivial relationship between $C_1^{(2)}$ and $\alpha^{(2)}$ is observed in Fig. 3 (b).

Figure 2 (b) shows that we obtain a different surface for each simulation condition of the ion temperature gradient R_0/L_{T_i} . The coefficients depend on the ion temperature gradient for Model12 defined in Eq. (7), namely $(C_1^{(2)}, C_2^{(2)}, \alpha^{(2)}) = (C_1^{(2)}[R_0/L_{T_i}], C_2^{(2)}[R_0/L_{T_i}], \alpha^{(2)}[R_0/L_{T_i}])$. It is also confirmed that the curved surface of Model11 intersects with each surface of Model12 around the average values of $\tilde{\chi}_i$.

We apply the results of Model12 to construct a model function for the ITG turbulent plasma transport. Assuming the error, σ as

$$\sigma = \sqrt{\frac{1}{n} \sum_{l=1}^n \left(\frac{\langle \tilde{\chi}_i^{\text{Model1}} \rangle_l}{\langle \tilde{\chi}_i^{\text{GKV}} \rangle_l} - 1 \right)^2}. \quad (9)$$

Here, the numbers l and n are the index number and the total number of the simulation conditions. The errors

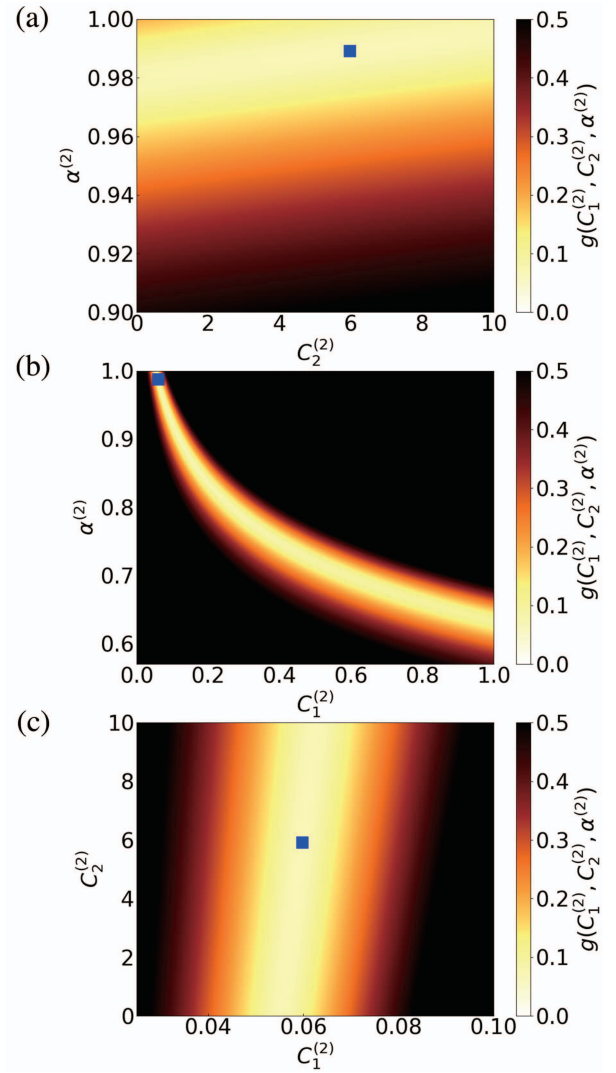


Fig. 3 Contours of $g(C_1^{(2)}, C_2^{(2)}, \alpha^{(2)})$ at (a) $C_1^{(2)} = 6.0 \times 10^{-2}$, (b) $C_2^{(2)} = 6.0$, and (c) $\alpha^{(2)} = 9.9 \times 10^{-1}$ for $R_0/L_{T_i} = 15.0$. The blue squares indicate the global minimum.

are for Model11, $\sigma_{\text{Model11}} = 1.7 \times 10^{-2}$ and for Model12, $\sigma_{\text{Model12}} = 1.0 \times 10^{-2}$. Therefore, as also shown in Fig. 4, the functional relation for time series data by Model12 achieves a higher reproduction accuracy than for time-averaged data by Model11.

4. Discussion

In Model12, Fig. 4 (b) shows a monotonically decreasing trend with increasing $\tilde{\chi}_i^{\text{GKV}}$ which is an unnatural trend. The objective function $g(C_1^{(2)}, C_2^{(2)}, \alpha^{(2)})$ defined in Eq. (8) is a major cause of the trend. If we define $\Delta\tilde{\chi}_i(t) = \tilde{\chi}_i^{\text{Model12}}(t) - \tilde{\chi}_i^{\text{GKV}}(t)$, we obtain following formulation from Eq. (8),

$$g(C_1^{(2)}, C_2^{(2)}, \alpha^{(2)}) = \sqrt{\frac{1}{N} \sum_{j=1}^N (\Delta\tilde{\chi}_i(t_j) / \tilde{\chi}_i^{\text{GKV}}(t_j))^2}.$$

Here, for a bigger denominator, the value of $\Delta\tilde{\chi}_i(t_j) / \tilde{\chi}_i^{\text{GKV}}(t_j)$ is estimated smaller. Since we consider the satu-

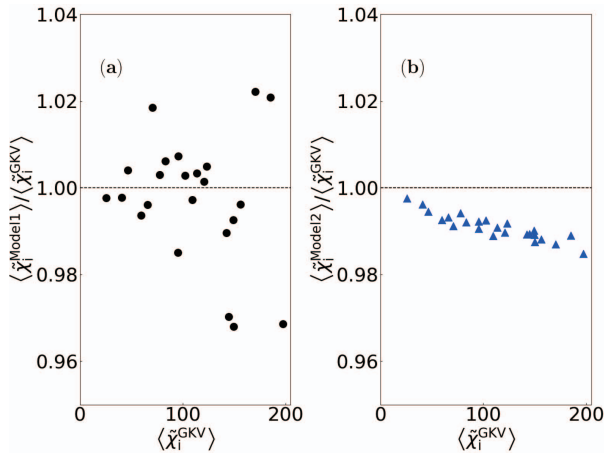


Fig. 4 Comparison of functional relation for (a) time averages and (b) time series data.

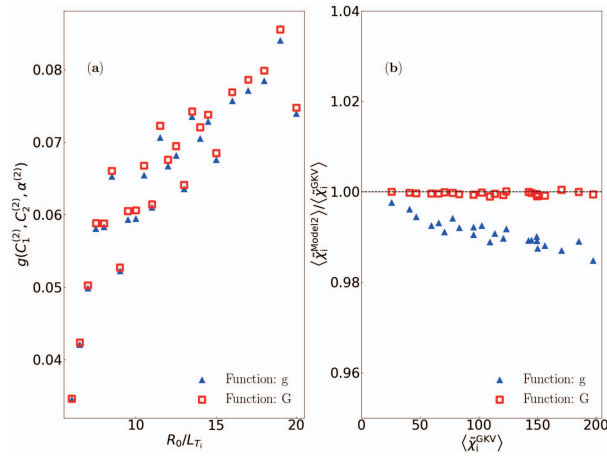


Fig. 5 Comparison of the value of the fitted results of (a) $g(C_1^{(2)}, C_2^{(2)}, \alpha^{(2)})$ and (b) $\langle \tilde{\chi}_i^{\text{Model12}} \rangle / \langle \tilde{\chi}_i^{\text{GKV}} \rangle$ for the case using $g(C_1^{(2)}, C_2^{(2)}, \alpha^{(2)})$ and $G(C_1^{(2)}, C_2^{(2)}, \alpha^{(2)})$.

rated part of the time series for each condition in this work, the fluctuation level is the same extent for each ion temperature gradient. Therefore, irrespective of $\tilde{\chi}_i^{\text{GKV}}(t)$, it is necessary to evaluate $\Delta\tilde{\chi}_i(t)$ at the same level for each simulation condition.

We introduce new objective function $G(C_1^{(2)}, C_2^{(2)}, \alpha^{(2)})$ defined by,

$$G(C_1^{(2)}, C_2^{(2)}, \alpha^{(2)}) = \sqrt{\frac{1}{N} \sum_{j=1}^N (\tilde{\chi}_i^{\text{Model12}}(t_j) - \tilde{\chi}_i^{\text{GKV}}(t_j))^2}. \quad (10)$$

Figure 5 shows the results with two different objective functions. For every ion temperature gradient, the value of $g(C_1^{(2)}, C_2^{(2)}, \alpha^{(2)})$ obtained by using itself as the objective function are below the case using $G(C_1^{(2)}, C_2^{(2)}, \alpha^{(2)})$, as shown in Fig. 5 (a). However, for the function G case, the reproduction of time-averages of $\tilde{\chi}_i$ is better than for

the function g case in Fig. 5 (b), $\sigma_G = 5.2 \times 10^{-4}$ and $\sigma_g = \sigma_{\text{Model12}} = 1.0 \times 10^{-2}$, respectively.

5. Conclusion

In this paper, we reported the existence of the structure of the time series data of gyrokinetic simulations in the parameter space of turbulences, zonal flows, and transport coefficients, and the application of the structures to transport modeling. Considering the functional relation for time series data of the turbulent amplitude, zonal flow amplitude, and transport coefficient, we obtain the time-dependent functional relation $\tilde{\chi}_i^{\text{Model12}}(t)$ for each simulation condition. The functional relation can reduce relative error which is compared with the previous function obtained by taking the time-averages. By examining the objective function, the new functional relation gets even better reproduction. The functional relation for the electron transport coefficients and the modeling in consideration of the electron temperature gradient, and the density gradient is also of interest, and will be investigated in the future.

Acknowledgments

We would like to thank Dr. M. Nakata, Dr. S. Matsuoka, and Mr. T. Nakayama for useful discussions. This work is supported in part by NIFS Grants (NIFS 20KNST161, NIFS21KNTS071), and JSPS KAKENHI (16H04620, 20K03907, 17K14899), and by MEXT as ‘‘Program for Promoting Researches on the Supercomputer Fugaku’’ (Exploration of burning plasma confinement physics, JPMXP1020200103). The simulations were performed by using the Plasma Simulator at the National Institution for Fusion Science, and JFRS-1 at IFERC-CSC.

- [1] W. Horton, Rev. Mod. Phys. **71**, 735 (1999).
- [2] X. Garbet, Y. Idomura, L. Villard and T.-H. Watanabe, Nucl. Fusion **50**, 043002 (2010).
- [3] R.E. Waltz, G.M. Staebler, W. Dorland, G.W. Hammett, M. Kotschenreuther and J.A. Konings, Phys. Plasmas **4**, 2482 (1997).
- [4] G.M. Staebler, J.E. Kinsey and R.E. Waltz, Phys. Plasmas **12**, 102508 (2005).
- [5] G.M. Staebler, J.E. Kinsey and R.E. Waltz, Phys. Plasmas **14**, 055909 (2007).
- [6] J.E. Kinsey, G.M. Staebler and R.E. Waltz, Phys. Plasmas **15**, 055908 (2008).
- [7] C. Bourdelle, X. Garbet, F. Imbeaux, A. Casati, N. Dubuit, R. Guirlet and T. Parisot, Phys. Plasmas **14**, 112501 (2007).
- [8] M. Nunami, T.-H. Watanabe and H. Sugama, Phys. Plasmas **20**, 092307 (2013).
- [9] T.-H. Watanabe and H. Sugama, Nucl. Fusion **46**, 24 (2006).
- [10] E.A. Frieman and L. Chen, Phys. Fluids **25**, 502 (1982).
- [11] S. Maeyama, A. Ishizawa, T.-H. Watanabe, N. Nakajima, S. Tsuji-Iio and H. Tsutsui, Comput. Phys. Commun. **184**, 2462 (2013).
- [12] J.A. Nelder and R. Mead, Comput. J. **7**, 308 (1965).